Comparative study of collision cascades and resulting displacement damage in GaN, Si and Ge

Julien Parize, Thomas Jarrin, Antoine Fées, Damien Lambert, Antoine Jay,
Valentin Morin, Anne Hemeryck, Nicolas Richard

HAL Id: hal-04542795

https://hal.science/hal-04542795v1

Submitted on 11 Apr 2024

Comparative study of collision cascades and resulting displacement damage in GaN, Si and Ge

Julien Parize, Thomas Jarrin, Antoine Fées, Damien Lambert *Senior Member, IEEE*, Antoine Jay, Valentin Morin, Anne Hemeryck and Nicolas Richard

Abstract—To assess the sensitivity of microelectronic devices to displacement damage, molecular dynamics simulations of collision cascades in GaN, Si and Ge are performed. We compare results on these three materials using a wide range of data coming from a very large amount of simulations. The statistical analysis of these data probes into the dynamics of cascades in terms of generating defects, the healing process, and the formation of defect clusters. In GaN, we observe that up to 90% of the defects created during a collision cascade initiated by a Ga atom disappear after a few tens of ps. In addition, the larger clusters tend to decrease rapidly in size. At the end, only small clusters remain in GaN, contrary to Si and Ge where large amorphous pockets are present. This metal-like in-cascade defect annealing seems to be closely related to the dense atomic structure of wurtzite GaN. Results confirm that GaN is intrinsically more resistant to non-ionizing radiation than Si and Ge at the studied energies, and over the considered timescales.

Index Terms—Gallium Nitride, Silicon, Germanium, Radiation, Displacement Damage, Molecular Dynamics, Defects, Clusters

I. INTRODUCTION

WHEN penetrating the materials constituting electronic and optoelectronic components, particles can interact with electrons and nuclei producing ionization through electron-hole pair generation and displacement damage (DD) respectively. Ionization can be quantified via the ionizing energy loss (IEL) and nuclei-nuclei elastic collisions producing DD via the non-ionizing energy loss (NIEL). In this paper, we focus on the latter contribution.

Following the non-ionizing interaction with an incident energetic particle, some ions are ejected from their equilibrium position. These moving ions interact with the electronic structure of the material and collide with neighboring nuclei, creating defects in the semiconductor layer of electronic devices by breaking the symmetry and periodicity of the crystalline structure. This succession of collisions can lead to a so-called collision cascade generating numerous defects.

The basic bricks of created defects are Frenkel pairs where an atom leaves its own lattice position and instead occupies a normally vacant site. This creates a point defect called a vacancy, *i.e.*, an empty crystalline lattice site, and a displaced lattice atom. The displaced atom may have an initial kinetic energy and is capable of further defect evolution, ending up as an interstitial, *i.e.*, an atom not located on a crystalline lattice site or, in multi-atom compounds, another important type of point defect, an antisite, *i.e.*, an atom of a type "i" in a crystalline lattice site of a type 'j'≠'i' atom.

Those defects can aggregate to form clusters. Also, complete amorphisation of the crystalline matter can be observed as shown in [1] and [2]. In silicon (Si), the created defects are known to have dramatic consequences in bipolar transistors [3] and complementary metal oxide semiconductor image sensors [4]. In the latter, the creation of defect energy levels in the Si band gap increases the thermal generation of charge carriers and results in an extra contribution of the output current called dark current [4].

In recent years, aiming at improving the efficiency of power and radio-frequency Si-based devices, interest has grown for gallium nitride (GaN), which exhibits remarkable properties [5] for these applications, such as a large band gap of 3.4 eV compared to 1.1 eV in Si, a high breakdown field of 3.3 MV/cm, compared to 0.3 MV/cm in Si. GaN also shows a remarkable temperature resistance [6]. Some studies reported that GaN devices can be very sensitive to DD [7]–[9]. However, the majority of studies investigating the response of GaN devices to DD have observed low sensitivity of the devices [10]. At the material level, the few studies carried out have proposed that the resistance of the devices could find its origin in the intrinsic properties of the GaN material. In [11], [12], Nord *et al.* used Molecular Dynamics (MD) to investigate the accumulation of damage during ion beam irradiation of GaN. Collision cascades initiated by Ga and N Primary Knock-on Atoms (PKA) between 200 eV and 10 keV are simulated. It is found that few thermally equilibrated defects are created in GaN. Also the number of defects created in the GaN material increases with temperature. Chen *et al.* have also performed MD simulations [13] with Ga PKAs ranging from a few hundreds of eV to 40 keV. They witness a large number of atoms being displaced during the defect peak of collision cascades, followed by a self-healing within the cascades, resulting in a small quantity of defects remaining only 20 ps after the beginning of the cascade. This drastic GaN picosecond scale in-cascade self-healing is similar to what can be observed in metals, but is very different from the known defect recombination dynamics occurring in Si, Ge, or GaAs [14], which take place on much longer timescales. This self-healing has also been observed very recently, both in MD

simulations and via transmission electron microscopy (TEM). In the case of defects created following Swift Heavy Ion (SHI) irradiation [15]. However, it has never been experimentally observed for collision cascades. Actually, there are very few TEM studies devoted to the structural analysis of collision cascades in semiconductors [16], [17], especially in GaN. Indeed, if the ion tracks produced by SHI irradiation are large enough to be imaged [15], due to the inherent thickness of the samples, the color contrast difference due to small clusters of defects produced in collision cascades are hard to identify even in high resolution TEM images.

It is to attain this atomic scale description necessary to investigate the presumed intrinsic resistance of GaN material to DD that, in this paper, we apply MD simulations.

To our knowledge, there is only one study taking into account N PKAs [11] in GaN, though N PKAs form a significant part of the created PKAs following neutron irradiation [18]. In the published literature on GaN collision cascades, a detailed analysis of the dynamics of the cascades in terms of defect creation and clustering is also lacking. Consequently, in this paper, we study collision cascades in GaN initiated with both Ga and N PKAs based on a larger number of simulations than previously done at three energy levels: 1 keV, 10 keV and 25 keV. Moreover, cascade dynamics are closely tracked and analyzed. In addition, to have a complete and clear idea of the relative sensitivity of GaN to non-ionizing radiation compared to other standard materials for microelectronics, results in GaN are compared to those obtained in Si and Ge.

The work conducted in this article is part of a larger effort to increase the fidelity of our understanding of DD effects, and to link atomic scale modeling and experiments to device-based observations. The methodology employed for achieving this has already been extensively described and applied to Si [19]–[22] and to some extent to Ge and Si-Ge alloys [23], [24].

We emphasize that our results represent a snapshot in time of the dynamic displacement damage effects that occur through collision cascades. After that moment in time at the end of the cascades, the ensemble of defects continues to evolve as a result of atomic diffusion and drift over an extended period of time. Those longer time effects are not included in this analysis.

II. METHODS

MD collision cascade simulations are conducted using the LAMMPS code [25]. MD allows the description of matter at the atomic scale and enables the dynamic study of collision cascades within a material. In MD, time is discretized, and at each timestep, the Newton equation of motion (1) is solved for each atom involved in the simulation:

$$m_i \frac{d\vec{v_i}}{dt} = \vec{F_i} \quad (1)$$

with m_i the mass of atom i, $\vec{v_i}$ its velocity and $\vec{F_i}$ the force acting on it. In order to update the velocity and position of atom i at each timestep, the force $\vec{F_i}$ acting on it must be known. In MD, this force can be analytically derived from interatomic potentials [26]. These potentials take the positions of each atom in the simulation as parameters, and compute the forces based on those positions.

Through MD simulations of collision cascades, we want to accurately simulate the ballistic aspects of the cascades, and also the structure and global properties of the material, since they have a major influence on the collision cascade, and on the resulting state of damage [27]. This is what makes MD more complete than the Binary Collision Approximation (BCA), in which only ballistic aspects are considered. In order to achieve this, an interatomic potential, calibrated according to experimental data, and able to reproduce at the same time general equilibrium properties of the material, such as structure, cohesive energy, melting temperature among other properties, and highly non-equilibrium high energy ion-ion collisions must be employed. In previous studies focused on Si [20], [24], the Stillinger-Weber (SW) potential was used. However, for GaN, its use was very limited and confined to structural studies [28]. Given that our objective is to compare the results obtained for GaN, Si and Ge starting from the same theoretical grounds, we choose to employ Tersoff potentials coupled to repulsive ZBL potentials [29] for Si [30], [31], GaN [11]–[13] and Ge [32]. For Ge, we had to define the coupling parameters for the purpose of this study. More details are given in the Supplementary Material.

In addition to the previously mentioned properties, it is necessary to include non-adiabatic electronic effects to have a complete picture of the process involved in the collision cascade. Thus, we incorporate the electronic stopping power [33] in our simulations by the insertion of a friction force in (1).

Our MD collision cascade simulations take place in boxes created from non-primitive orthorhombic unit cells composed of 8 sites (4 Ga and 4 N) for which the lattice parameters are a = 3.18 Å, b = 5.52 Å and c = 5.17 Å. To create the Si and Ge simulation boxes, we use a diamond unit cell composed of 8 atoms and for which the lattice parameters are a_{Si} = 5.43 Å and a_{Ge} = 5.66 Å. Different types of PKAs are employed (both Ga and N in GaN, Si in Si, Ge in Ge), with energies of 1, 10, 25 keV. Due to the large difference in the size of the cascades depending on the PKA types, we use simulation boxes of different sizes: for 1 keV PKAs, box sidelengths range from 150 Å to 200 Å, *i.e.*, from 294 408 to 659 680 atoms, for 10 keV PKAs, box sidelengths range from 300 Å to 600 Å, *i.e.*, from 2 398 880 to 19 016 576 atoms, for 25 keV PKAs, boxes sidelengths range from 400 Å to 1000 Å, *i.e.*, from 4 096 000 to 88 031 160 atoms.

The system is equilibrated for 20 ps at 300 K with a timestep of 1 fs before the initiation of the collision cascade. Collision cascades are started by attributing to an atom, chosen as the PKA, a certain velocity vector corresponding to the desired PKA energy. For each PKA type and each energy, 100 simulations are run, each one with a different direction in order to obtain statistically relevant results [34]. The timestep is chosen based on the distance covered by the PKA between two timesteps, which does not exceed 0.025 Å in our simulations. Additional detail about the chosen integration ensembles and thermostat can be found in [24]. The maximum penetration

depth of the PKA, the number of created defects and the spatial distribution, diffusion and clustering of defects are analyzed.

The number of defects is defined as the number of Frenkel pairs (number of interstitial-vacancy pairs created). There exists different methods for counting defects, for example the Lindemann criterion [35], previously used [23]. For Si and Ge materials, the Lindemann and Wigner-Seitz methods are known to give different absolute results but to scale very well [27]. In this article, we chose to calculate the number of defects with the Wigner-Seitz criterion [36], implemented in OVITO. Data processing is performed using OVITO visualization software and its analysis tools [37].

Considering that a quantitative comparison of our results with experimental results is difficult to achieve, in the following, our results are compared with simulations performed with the Transport and Range of Ions in Matter (TRIM) program [38], which is part of the Stopping and Range of Ions in Matter (SRIM) tool. TRIM simulations are based on the BCA, and matter is described as a continuous medium. Therefore, certain effects that can be captured with MD (for example temperature influences), and structure related information (clustering of defects for example) are not accessible with TRIM. Therefore, all our results cannot be compared to TRIM. However, extensive calibration and comparison of TRIM/SRIM with experimental stopping power and ion range results makes it a trustworthy comparison point and a reliable reference for MD simulations, especially for the range of the ions in matter, which are compared to the maximum penetration depth we report.

III. Results

For all the studied materials, and all the investigated energies, cascades are simulated for 22.6 ps. In the following, the term "end" refers to the material structure at the end of the simulations, *i.e.*, after 22.6 ps. The peak of the cascade designates the moment of the simulation at which the maximum number of defects is attained. The number of defects represents the number of interstitial-vacancy pairs. The size of a cluster designates the number of vacancies, interstitials and/or antisites (for GaN only) it contains. Two constituents (interstitials, vacancies or antisites) belong to the same cluster if they are separated by less than twice the nearest neighbor distance. In this section, results for all energies are included in Table I and II but for the sake of conciseness, only graphs with PKAs of 10 keV are shown. Graphs for the other studied PKA energies, *i.e.*, 1 keV and 25 keV, are given in supplementary materials.

A. State of damage at the end of the simulations

Figure 1 shows the maximum penetration depth distribution of PKAs at 10 keV for Ga and N PKAs in GaN, Si PKAs in Si and Ge PKAs in Ge based on 100 MD simulations for each case. The average values of both the maximum penetration depth and the number of defects for 10 keV cascades are summarized in Table I, alongside the average values for 1 keV and 25 keV cascades as well. Following Fig. 1, for Ga PKAs in GaN, the penetration depth distribution is very homogeneous,

with more than 90% of the simulated cascades having a depth between 10 and 100 Å. On the contrary, for N PKAs, the distribution seems very dispersed, ranging from a few Å to more than 400 Å, with an average depth of 234 Å, much deeper than that of Ga PKAs (56 Å). In agreement with our previous studies on the subject, Si PKAs penetrate deeper than Ge PKAs [23]. Figure 1 reveals that Si PKAs also penetrate a lot deeper than Ga PKAs, but far less than N PKAs. Ge and Ga PKAs display a similar distribution of their range of penetration. The average values of Table I show that the same trend can be observed at 1 keV and 25 keV. This is also confirmed by Figs. S1 and S2, showing the same data as Fig. 1 but for 1 keV and 25 keV PKAs. These wide differences in penetration can be explained by the difference in terms of mass and size of PKA but also in terms of disparities in the density of each materials, *i.e.*, $\rho_{GaN} = 6.15$ g/cm^3, $\rho_{Si} = 2.33$ g/cm^3 and $\rho_{Ge} = 5.32$ g/cm^3.
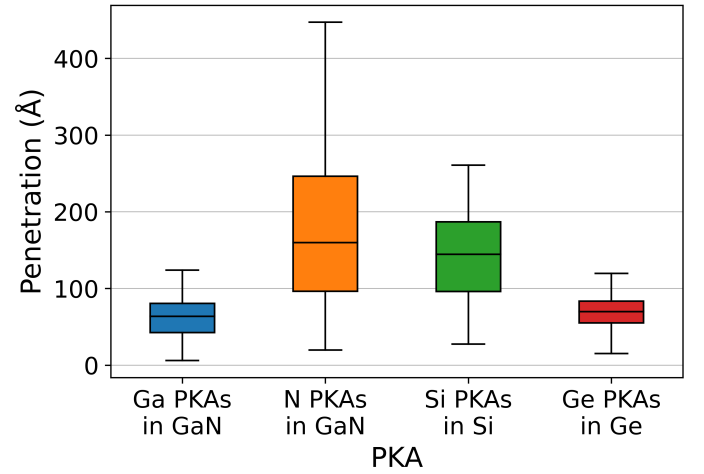

Fig. 1. Box plots of the maximum penetration depth of Ga PKAs in GaN (blue), N PKAs in GaN (orange) , Si PKAs in Si (green) and Ge PKAs in Ge (red) for 10 keV collision cascades. From lowest to highest, the horizontal lines of a box plot represent the minimum value of the set, the first quartile value, the median, the third quartile, and the maximum value of the set.

Figure 2 shows the distribution of the number of defects obtained at the end of simulations of 10 keV collision cascades initiated by Ga and N PKAs in GaN, Si PKAs in Si and Ge PKAs in Ge. Large differences between the three materials can be also observed here.

The distributions of the number of defects in GaN are considerably lower than in Si and Ge: between 30 and 60 for Ga PKAs in GaN, 20 and 50 for N PKAs in GaN compared to between 150 and 230 for Si PKAs in Si and between 180 and 320 for Ge PKAs in Ge. The drastic difference between the three materials is made even clearer in Table I: the mean number of defects in Ge (243) and Si (185) is about five times and four times that in GaN for Ga and N PKAs (42 and 36 respectively).

In addition to the observed discrepancies, it is also striking that cascades initiated by Ga PKAs and N PKAs tend to generate very similar numbers of defects (mean values of 45 for Ga PKAs and 36 for N PKAs). Indeed, previous studies showed that the numbers of defects after a collision cascade

TABLE I
COMPARISON TABLE OF AVERAGE MAXIMUM PENETRATION DEPTH AND AVERAGE NUMBER OF DEFECTS AFTER 1 keV, 10 keV AND 25 keV COLLISION CASCADES INITIATED BY Ga PKAs IN GaN, N PKAs IN GaN, Si PKAs IN Si AND Ge PKAs IN PKA. STANDARD DEVIATIONS ARE SHOWN IN PARENTHESIS. TRIM DISPLACEMENT ENERGY THRESHOLDS ARE : ED_{Ga}: 25 eV, ED_N: 28 eV, ED_{Si}: 15 eV, ED_{Ge}: 15 eV.

Energy	Data	Method	*Ga*	*N*	*Si*	*Ge*
1 keV	Penetration depth (Å)	MD	20 (8)	26 (15)	29 (16)	22 (12)
		TRIM	19	30	36	23
	Interstitials	MD	5 (2)	4 (2)	22 (3)	22 (3)
		TRIM	12	9	19	22
10 keV	Penetration depth (Å)	MD	65 (32)	177 (106)	133 (38)	65 (40)
		TRIM	63	180	181	84
	Interstitials	MD	42 (7)	36 (8)	185 (18)	243 (35)
		TRIM	116	84	171	208
25 keV	Penetration depth (Å)	MD	112 (55)	413 (183)	323 (140)	129 (56)
		TRIM	118	393	402	160
	Interstitials	MD	105 (11)	71 (12)	403 (45)	640 (106)
		TRIM	281	178	384	502

in binary materials can vary greatly depending on the type of PKA, notably in Si-Ge alloys [23], [39]. Figures S3 and S4 which show the box plots of the number of defects for 1 keV and 25 keV cascades confirm the trends derived from Fig. 2. Also, at all the considered energies, Ga and N PKAs tend to generate very similar numbers of defects.

To analyze in more detail the created defects in GaN, Table II displays for all the considered PKA energies the average number of each defect type (interstitial, vacancy, antisite), as a function of the atom type. At all energies, antisites are the minority defects. We find no clear trends regarding the dominance of Ga interstitials or N interstitials (or vacancies). Indeed, we observe that for N PKAs, at 1 keV and 10 keV, more Ga interstitials are created, whereas the inverse is observed for Ga PKAs at all energies. Also, at 10 keV and 25 keV, regardless of the PKA type, there are more Ga vacancies.
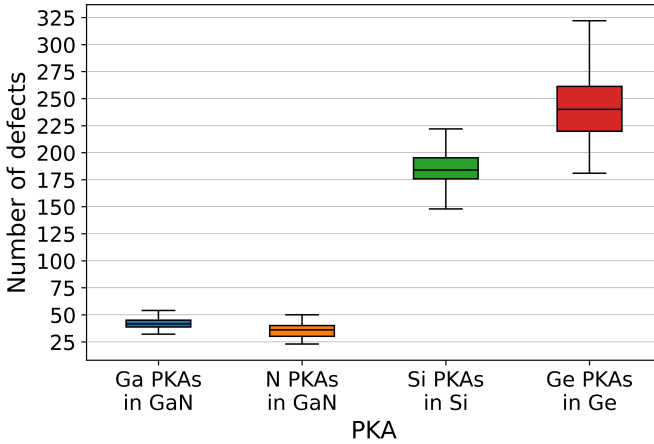

Fig. 2. Box plots of the number of defects after 10 keV collision cascades initiated by Ga PKAs in GAN (blue), N PKAs in GaN (orange), Si PKAs in Si (in green) and Ge PKAs in Ge (in red). From lowest to highest, the horizontal lines of a box plot represent the minimum value of the set, the first quartile value, the median, the third quartile, and the maximum value of the set. One hundred simulations are run for each type of PKA.

Alongside the mean values derived from MD, Table I contains the average maximum penetration depth and average number of defects obtained from TRIM after 1 keV, 10 keV

and 25 keV collision cascades initiated by Ga and N PKAs in GaN, Si PKAs in Si and Ge PKAs in Ge. The averages obtained using TRIM are calculated based on the results of 5000 simulations. Absolute values of penetration depth are in very good agreement between MD and TRIM for Ga and Ge PKA. For N and Si PKA penetration depths, quite important discrepancies are observed (about 50 Å). The trends identified with MD are verified with TRIM, except in the case of Si and N PKAs, for which MD predicts a 40 Å discrepancy at 10 keV between the two mean penetration depth values, whereas TRIM predicts nearly no difference between the two, whatever the energy.

Concerning the total number of defects, the absolute values are hardly comparable between the two methods. Indeed, both methods are so different in their nature, that the values given by the method for counting defects in both cases cannot really be set side by side. However, the trends in the evolution in the number of defects depending on the PKA types and materials can be analyzed and compared. On the whole, for all energies, the average number of defects globally follows the same trends between the two simulation methods, a Si PKA in Si or a Ge PKA in Ge generates more defects than Ga and N PKAs in GaN, with slightly more defects in GaN in a collision cascade initiated by a Ga PKA. In more detail, with MD, at 10 keV it is observed that about 5 times fewer defects are created by a Ga PKA in GaN and a N PKA in GaN than a Si PKA in Si and about 6 times fewer defects created than a Ge PKA in Ge. With TRIM, at 10 keV, only about 2 times fewer defects are observed for Ga and N PKAs in GaN compared to Si and Ge. The trends thus are not completely similar, as TRIM tends to overestimate the number of defects created in GaN and underestimates the number of defects in Si and Ge compared to MD simulations. The reasons for this underestimation will be discussed in section IV.

B. Collision cascade dynamics and clustering

We focused in the previous paragraph on the final state of the cascades only, but MD allows us to explore not only static pictures but also the dynamic evolution of the cascades. Figure 3 shows the evolution of the number of defects over the entire MD simulation time, for 10 keV collision cascades

TABLE II

PER ATOM TYPE AVERAGE NUMBER OF INTERSTITIALS (I_{Ga} AND I_N), VACANCIES (V_{Ga} AND V_N) AND ANTISITES (Ga_N AND N_{Ga}) IN 1 keV, 10 keV AND 25 keV GaN COLLISION CASCADES INITIATED WITH N AND Ga PKAS. STANDARD DEVIATIONS ARE GIVEN IN PARENTHESIS.

	I_{Ga}	I_N	V_{Ga}	V_N	Ga_N	N_{Ga}
N PKA in GaN						
1 keV	2 (1)	2 (1)	2 (1)	2 (1)	1 (1)	1 (1)
10 keV	19 (4)	18 (4)	21 (4)	15 (4)	5 (3)	3 (2)
25 keV	33 (12)	36 (13)	42 (12)	27 (13)	10 (5)	7 (4)
Ga PKA in GaN						
1 keV	2 (1)	4 (1)	1 (1)	5 (1)	2 (1)	0 (1)
10 keV	20 (4)	23 (4)	23 (4)	19 (4)	8 (2)	6 (2)
25 keV	47 (6)	59 (9)	57 (6)	49 (8)	18 (4)	13 (4)

Fig. 3. Defects number evolution profile during 22.6 ps for 10 keV collision cascades initiated by Ga PKAs in GaN (blue o), N PKAs in GaN (orange △), Si PKAs in Si (green x) and Ge PKAs in Ge (red |). Defect data are derived from averaging results across 100 simulations for each respective case.

initiated by Ga and N PKAs in GaN, Si PKAs in Si and Ge PKAs in Ge. Each data point in Fig. 3 results from an average over the 100 performed MD simulations. A collision cascade can be divided in multiple steps. First, the ballistic phase occurs, during which fast moving Secondary Knock-On Atoms (SKAs) are created following collisions with the PKA. Those SKAs then create slow moving atoms and defects in the materials. Those steps correspond to the increasing part of Fig. 3. After a peak at which the maximum number of defects is reached, heat excess is evacuated and the material starts to recrystallize/heal. This step is sometimes called annealing. In all four cases, the cascades reach their maximum number of defects after a few tenths of a picosecond. The peak is reached more quickly in Si cascades (0.25 ps), then a little bit later for the N in GaN PKAs (0.30 ps) and the Ge in Ge PKAs (0.38 ps), and afterwards for the Ga in GaN PKAs (0.43 ps).

However, we observe very distinct behaviours in terms of the evolution of the number of defects between the different materials and PKAs. For 10 keV cascades, in GaN, the N PKAs produce cascades with a peak of less than 200 defects, in contrast to the Ga PKAs cascades which have a considerably higher peak of more than 575 defects. At the end of the simulations, the number of defects at 10 keV is only about 50 in Ga PKAs cascades, compared with 575 at the peak of those same cascades, *i.e.*, a reduction of 93%. For N PKAs, the reduction is 83% (from 208 to 36 defects). In GaN, cascades initiated by both Ga PKAs and N PKAs tend to almost entirely heal on their own. In Si, at 10 keV, the peak number of defects is of nearly 400 and that for Ge cascades is of about 500 defects. Although at the peak of the cascades in Si and Ge a lower number of defects is created than in GaN with Ga PKAs, the Si and Ge cascades end with a far greater number of defects (about 200 for Si and 250 for Ge, compared to 50 for GaN at 10 keV). The recrystallization is a lot more efficient and faster in GaN than in Si and Ge. This is what explains the very low number of defects found in GaN. The same trend can be observed for the other studied energies, and is even made more blatant in S6 which displays the evolution of the number of defects at 25 keV. Figure 4 shows the distribution of the number of clusters as a function of their size (number of defects) at the peak of 10 keV collision cascades and at the end of same collision cascade simulations in GaN (PKAs Ga and N), Si and Ge. In Si and Ge, clusters are defined as aggregates of vacancies and interstitials, and in GaN, as aggregates of vacancies, interstitials and antisites.
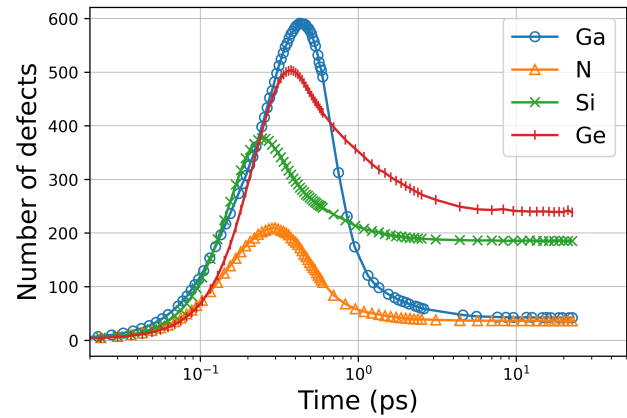
At the peak of the cascades, very large clusters are present in Ge, and even more in GaN in which regardless of the PKA type, clusters of more than 10^3 defects are observed. In Si, the clusters are smaller, not exceeding 500 defects. For all materials, at the peak of the cascade and at the end, the point defects are the dominant type of defects. Also, the smaller the size of the cluster, the more frequently it is observed. The largest cluster sizes mentioned above are rarely observed. The most interesting features of Fig. 4 are the evolutions between the distribution of clusters between the peak and the end. For all materials, a recrystallization is observed, as already shown Fig. 3. From the cluster point of view, it is characterized by a reduction of the number of clusters, and a reduction of the size of the clusters, with the end distributions of Fig. 4 shifting to the left compared to the peak ones. The average number of clusters at the peak of a cascade in GaN initiated by a Ga PKA is 26, which reduces to an average of 15 at the end of the same cascade simulation. Similarly, for N PKAs in GaN, the average cluster number is 26 at the peak, decreasing to an average of 13 clusters at the end of the same cascade simulations. In Ge, the average number of clusters at the peak of a cascade reaches 50, dropping to an average of 43 at the end of the same cascades. For Si, the peak cluster count is 55, which averages at 47 clusters at the end of the simulation of the same cascades. Those numbers tell us that a lot more clusters are formed in Si and Ge compared to GaN. Moreover, it can be easily noticed in Fig. 4 that the recrystallization and cluster number decrease is far more important in GaN than in Si and Ge. Indeed, the peak and end distributions of clusters are still overlapping for Si and Ge, while they are almost completely distinct in the case of GaN, regardless of the PKA, meaning that the clusters have considerably healed. At the peak of the cascade, the bigger clusters are observed in GaN, whereas at the end, the bigger are found in Ge (above 100 in size) and Si (nearly 100 in size). At the end of the simulations, in GaN, clusters do not exceed 20 in size. This highlights the nature of the strong recrystallization in GaN: big clusters disappear and turn into small ones.

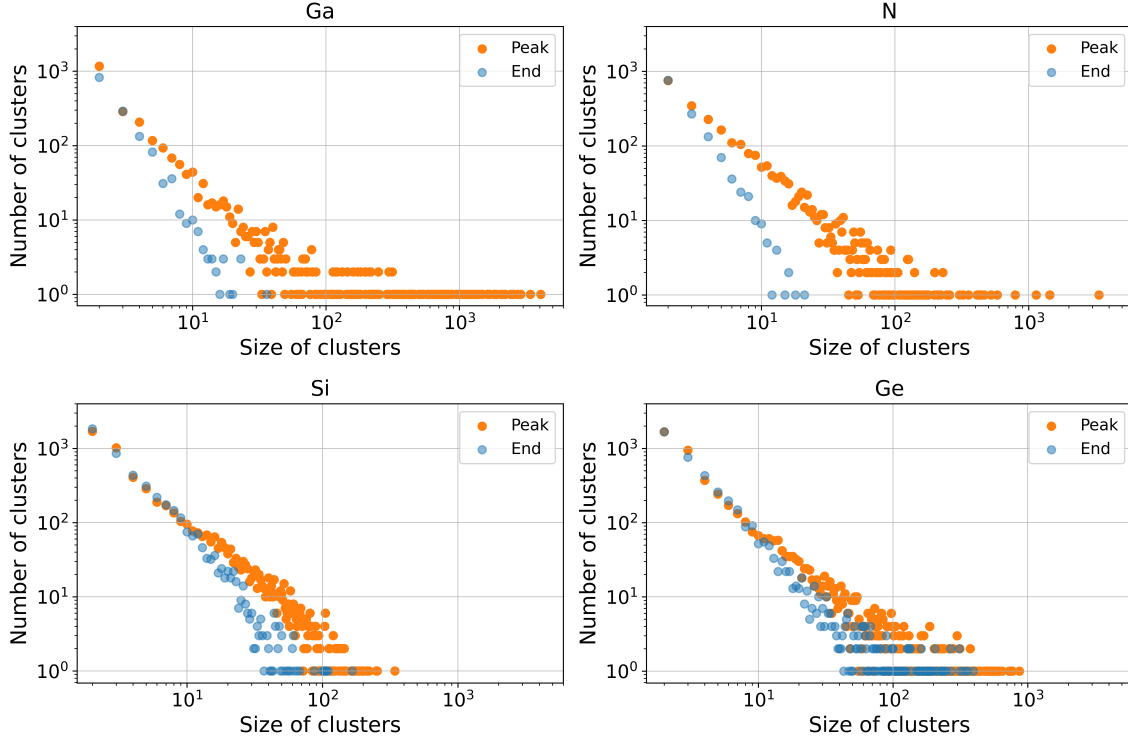Figure 5 exhibits a visual representation of defects clusters

Fig. 4. Distribution of the number of clusters as a function of their size at the peak of the 10 keV collision cascade (orange dots) and at the end of the same collision cascade simulation (blue dots). Ga PKAs in GaN (top left), N PKAs in GaN (top right), Si PKAs in Si (bottom left) and Ge PKAs in Ge (bottom right). Data are obtained from 100 simulations in each case.

at the peak and at the end of a 10 keV collision cascade simulation, initiated by a Ga PKA in GaN, a N PKA in GaN, a Si PKA in Si and a Ge PKA in Ge. The selected cascades in Fig. 5 are representative of average cascades for each PKA. They have been chosen because their average penetration depth and average number of defects closely align with the data provided in Table I. Notably, all four cascades share the same direction. Figure 5 provides a complementary visual representation of the cascades at 10 keV in the different materials. It is made clear that in GaN, the defects present at the peak have almost all disappeared at the end, whereas a lot more remain in Si and Ge. Also, it can be seen that for the Ga PKA case, the remaining clusters are of small size, whereas big clusters are still present in Si and Ge. The cascades shown in Fig. 5 correspond to average cascades; therefore, they do not encompass the full diversity of all possible cascade natures. This is for example why in the case of N PKAs in GaN, no big clusters can be seen though some are present in the pool of the 100 simulations carried out according to Fig. 4. However, it gives a fairly good visual representation of the cascade nature in each material and of the evolution of the created clusters of defects: at the peak, cascades are dense and localized in Ge and in GaN with Ga PKA, with many defects; dispersed in Si with clusters of all sizes; dispersed with mainly small clusters in GaN with N PKAs, whereas at the end, only small clusters remain in GaN; dispersed medium clusters in Si and dense big clusters in Ge.

IV. DISCUSSION

In the Results section, we have observed that the quantity and the characteristics of the defects formed can significantly vary depending on the material and the PKA types. As evidenced in Fig. 4 and Table I, in GaN, only a small number of defects remain at the end of cascade simulations, regardless of the PKA type. Also, the type of PKA has nearly no influence on the total number of defects created at the end. However, the spatial distribution of the defects varies depending on the PKA type, lighter and smaller PKAs tend to result in more dispersed cascades. In the cases of Si and Ge, defects are sometimes contained in very large amorphous clusters, and the number of defects surpasses that in GaN. On a macroscopic scale, the much higher melting temperature in GaN ($T_{GaN} \approx 2800$ K) than in silicon ($T_{Si} \approx 1700$ K) and germanium ($T_{Ge} \approx 1200$ K) [40], may explain those discrepancies. Indeed the low melting temperatures of Si and Ge allows the formation of amorphous zones of defects, well known in semiconductors after irradiation [41], whereas in GaN, it protects the material from the development of such amorphous pockets. This aspect is enhanced by the high thermal conductivity of GaN (1.3 W/cm·K [42]). However, following Fig. 3, the peak number of defects for a Ga PKA in GaN is even higher than in the case of Ge, meaning that the difference between the two materials comes from the recrystallization stage. This aspect can also be linked to the thermal properties. Lots of atoms are displaced by a Ga PKA in GaN, in a dense area (Table I), but the temperature attained

This article has been accepted for publication in IEEE Transactions on Nuclear Science. This is the author's version which has not been fully edited and content may change prior to final publication. Citation information: DOI 10.1109/TNS.2024.3380674
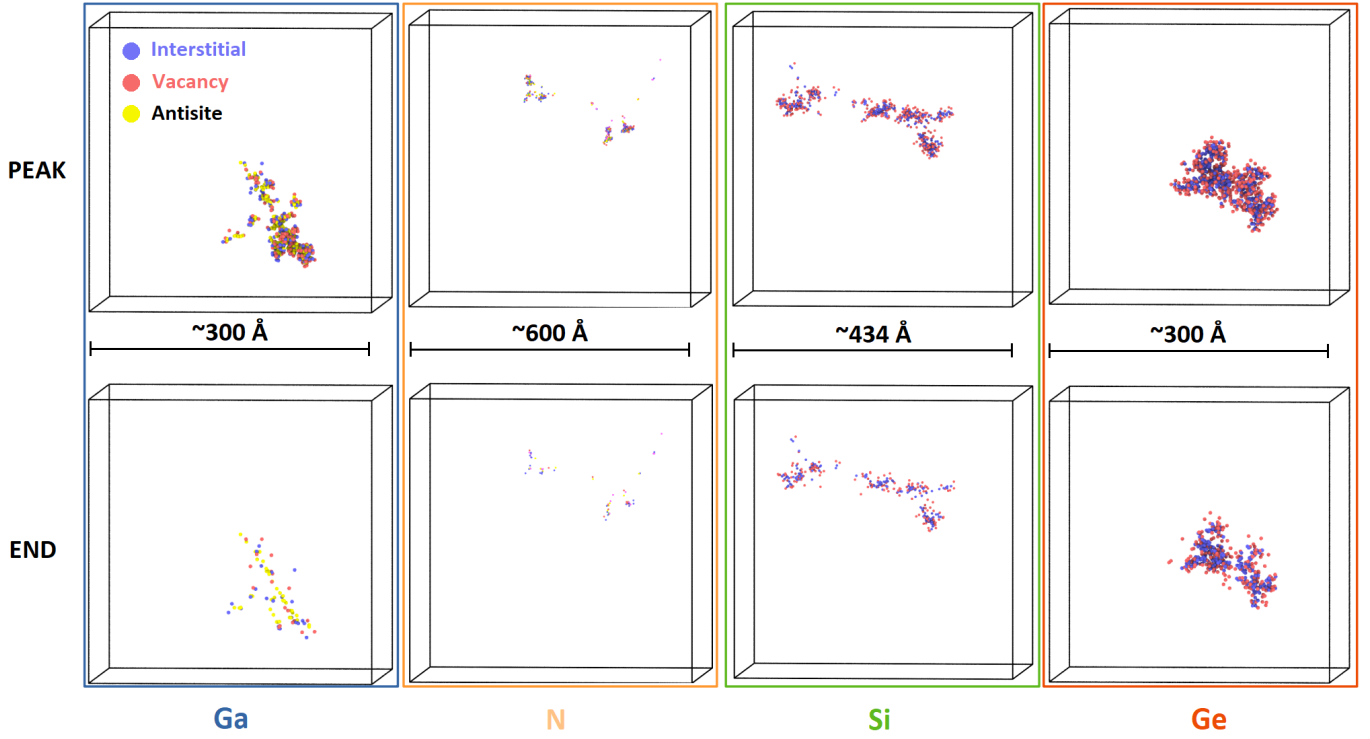
7

Fig. 5. Visual representation of defect clusters at the peak of a 10 keV collision cascade (top images) and at the end of the same 10 keV collision cascade simulation (bottom images) in GaN (PKAs Ga and N), Si and Ge. The blue spheres represent interstitial atoms, the red spheres represent vacancies and the yellow spheres represent antisites without specifying the type (Ga in an N site or N in a Ga site).

may not be high enough or does not hold for a sufficient time to melt the material and create amorphous pockets. Consequently, it leads to the healing of those displaced atoms. From an atomic scale perspective, according to [11], the threshold displacement energy (TDE) of Ga and N atoms in GaN ($E_d^{Ga} \approx 45$ eV and $E_d^{N} \approx 109$ eV) are higher that for Si in Si and Ge in Ge diamond structure ($E_d^{Si} = 20-35$ eV) [43], ($E_d^{Ge} = 23$ eV) [44]. This also offers an explanation for the greater resistance of GaN compared to Si and Ge. Also, the TDE is defined as the minimum energy to create a stable Frenkel pair. At lower TDE values than that given for GaN, atoms can be displaced for a short time, and thus be considered as interstitials, but will go back to their equilibrium position. This is very similar to what we observe in Figs. 3 and 4 in GaN. Lots of defects are created at the peak of the cascade, but the material recrystallizes and only a few defects remain in the end.

Going deeper in the atomic scale analysis, Fig. 6 displays the distribution of the distance the interstitials identified at the peak of the cascade are displaced from their initial equilibrium position (called displacement), at the peak of the cascade and at the end of the simulation. Therefore, the displacements plotted at the end are not all coming from interstitial atoms as many of the atoms identified as interstitials at the peak of the cascade are back to their initial position at the end of the simulation. The comparison of the peak curves of Fig. 6 reveals interesting features. In GaN, only one very strong peak arises at about 1.2 Å. In Si (Ge), two peaks can be clearly identified, at about 2.3 Å (2.4 Å) and 4.9 Å (5.4 Å); At the

peak of the cascade, interstitials have traveled further in Si and Ge than in GaN. Looking at the end (blue) curves of Fig. 6 tells us about the evolution of the atoms identified as interstitials. In Si and Ge, several peaks are clearly visible. The first peak near 0 Å corresponds to the part of the interstitials that healed and went back to their equilibrium position. A second peak can be identified, at the first nearest neighbour distance (2.35 Å for Si, 2.45 Å for Ge). A peak at the second-neighbor distance is almost noticeable. Those peaks correspond to interstitial atoms that found their place in the crystal in ejecting other atoms from their equilibrium position. In GaN, two very large peaks are clearly visible. The first one by 0 Å, just like for Si and Ge. The second one corresponds to the second nearest neighbour distance of the GaN material, which indicates that a proportion of the displaced atoms have shifted to the distance of the second nearest atom. The largest peak is close to 0 Å, indicating that a large proportion of the displaced atoms have returned to their original crystal sites, i.e., healing the material. This peak is much more prominent in GaN than in Si and Ge, which justifies the greater recrystallization. Finding precise atomic displacement distances corresponding to the distance between the first neighboring atom and the second neighboring atom links the displacement dynamics to the crystallography of the material. The manner in which Ga and N atoms are ordered in GaN, and the way they move in the crystal, explains the high degree of recrystallization present in this material, in contrast to Si and Ge. The atoms making up the clusters formed in GaN are thus displaced close to their original crystalline site, promoting healing, i.e., their return to their crystalline site,
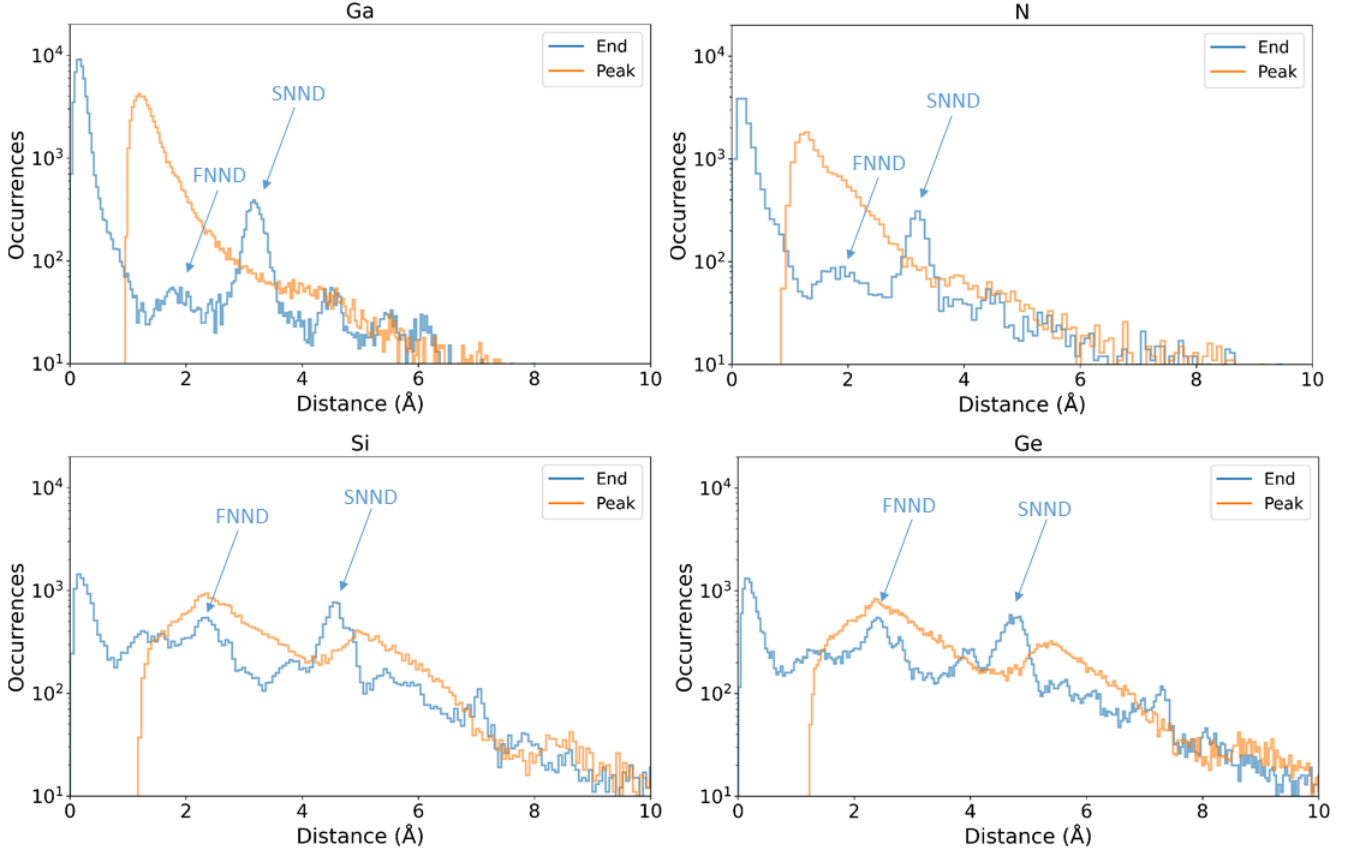
Fig. 6. Distributions of the distance the interstitials identified at the peak of the 10 keV cascades in GaN, Si and Ge are displaced from their initial equilibrium position (called displacement), at the peak of the cascades and at the end of the simulations. The first blue arrow represents the first nearest neighbour distance (FNND), the second represents the second nearest neighbour distance (SNND). Data are obtained from the average of 100 simulations in each case. At the peak of the cascades, the atoms selected to plot the displacements are all interstitials, whereas at the end, atoms identified as interstitials at the peak may have healed back to their initial position, and are thus not all interstitials.

thus reducing the number of defects and the number/size of clusters (Refer to Fig. 4)). The overestimation by TRIM of the number of defects created in GaN compared to in Si and Ge (see part I) can also be explained by the recrystallization characteristics of GaN. TRIM uses the BCA, which simplifies the picture of collision cascades by considering only two-body interactions (collisions). Atoms are represented as hard spheres that cannot interact directly with other atoms outside of collisions. On the contrary, MD, as it takes into account manybody interactions between all the atoms in the system (see part II) can be used to simulate complex behaviors such as melting, amorphization and defect and clusters reordering. Therefore, it is no surprise to observe discrepancies between MD and TRIM results when studying collision cascades in GaN, where complex recrystallization phenomena taking their origin in the thermal properties as well as in the crystal structure of GaN occur.

V. CONCLUSION

To better understand the effects of radiation-induced displacement damage in GaN, we ran 100 simulations for each collision cascade, at three different energies, 1 keV, 10 keV and 25 keV, in GaN, Si and also in Ge, for comparison. The behavior of the different PKAs and the three materials proved to be very different. N PKAs penetrate deeper into GaN than Ga PKAs and create a lot fewer defects at the peak of the cascade, *i.e.*, at the moment of the cascade when the maximum number of defects is reached. However, at the end of the simulations, a very similar number of defects is obtained with Ga and N PKAs in GaN. In Si and especially in Ge, a lot of defects are formed at the peak, but less than in GaN with Ga PKAs. Nonetheless, at the end, more defects remain in Si and Ge than in GaN, regardless of the PKA type. The clustering of the defects is also very different between the materials and the PKAs employed. In Ge, and in GaN with Ga PKAs, the concentration of defects is very dense at the peak. However, at the end, only a few defects remain in small clusters in GaN, whereas lots of defects mostly contained in large amorphous pockets are present in Ge. In Si, defects are contained in clusters of various sizes, including amorphous pockets, and dispersed along the trajectory of the PKA, which is longer than in Ge and in GaN with Ga PKAs. In GaN with N PKAs, the clusters obtained at the end are very few in number, and of very small size. Also, they are widely dispersed along the N PKA trajectories. Those intriguing observations come from the remarkable self-healing properties of the GaN material. Indeed, the number of defects dramatically and quickly decreases after the peak is reached.

Also, the distribution of the cluster size changes a lot between the peak and the end of the cascades, compared to Si and Ge. If very big clusters are present at the peak in GaN, they quickly heal, and in the end, only small clusters remain. Our study thus confirms, at the considered energies, the enhanced intrinsic resistance of GaN to displacement damage, compared to other semiconducting materials. We attribute the strong dynamic self-healing of GaN to its thermal properties, less favorable than Si and Ge for the formation of amorphous pockets, and also to very compact atomic structure of wurtzite GaN. Indeed, due to the small interatomic distance in GaN, interstitials rarely travel far from their equilibrium site, and are thus able to easily go back to their initial site, thus healing the structure. As part of our research initiative, we have planned irradiation experiments on bulk materials (Si and later GaN) and their characterization using a transmission electron microscope. The aim will be to compare the results of our simulations with the defects observed under the microscope in the samples tested.

REFERENCES

[1] A. Baba *et al.*, "Behavior of radiation-induced defects and amorphization in silicon crystal," *Nucl. Instr. Meth. Phys. R. A*, vol. 121, no. 1, pp. 299–301, Jan 1997.

[2] A. N. Larsen, "MeV ion implantation induced damage in relaxed $Si_{1-x}Ge_x$," *J. App. Phys.*, vol. 81, no. 5, pp. 2208–2218, Mar 1997.

[3] J. R. Srour, C. J. Marshall, and P. W. Marshall, "Review of displacement damage effects in silicon devices," *IEEE Trans. Nucl. Sci.*, vol. 50, no. 3, pp. 653–670, Jun 2003.

[4] J. M. Belloir *et al.*, "Dark current spectroscopy on alpha irradiated pinned photodiode CMOS image sensors," *IEEE Trans. Nucl. Sci.*, vol. 63, pp. 2183–2192, Aug 2016.

[5] I. Vurgaftman and J. R. Meyer, "Band parameters for nitrogen-containing semiconductors," *J. App. Phys.*, vol. 94, no. 6, pp. 3675–3696, Sep 2003.

[6] D. Maier *et al.*, "Testing the temperature limits of GaN-based HEMT devices," *IEEE Trans. Dev. Mat. Rel.*, vol. 10, no. 4, pp. 427–436, Dec 2010.

[7] F. Berthet *et al.*, "Influence of neutron irradiation on electron traps existing in GaN-based transistors," *IEEE Trans. Nucl. Sci.*, vol. 63, no. 3, pp. 1918–1926, Jun 2016.

[8] L. Lv *et al.*, "Significant degradation of AlGaN/GaN high-electron mobility transistors with fast and thermal neutron irradiation," *IEEE Trans. Nucl. Sci.*, vol. 66, no. 6, pp. 886–891, Feb 2019.

[9] M. A. J. Rasel *et al.*, "Heavy ion irradiation induced failure of gallium nitride high electron mobility transistors: effects of in-situ biasing," *J. App. Phys.*, vol. 56, no. 30, May 2023, Art. no. 305104.

[10] S. J. Pearton *et al.*, "Review of radiation damage in GaN-based materials and devices," vol. 31, no. 5, Sep 2013, Art. no. 050801.

[11] J. Nord *et al.*, "Molecular dynamics study of defect formation in GaN cascades," *Nucl. Instr. Meth. Phys. R. B*, vol. 202, pp. 93–99, Apr 2003.

[12] J. Nord, *et al.*, "Modelling of compound semiconductors: analytical bond-order potential for gallium, nitrogen and gallium nitride," *J. Phys.: Cond. Matter.*, vol. 15, no. 32, pp. 5649–5662, Aug 2003.

[13] N. Chen *et al.*, "Atomic-scale simulation for pseudometallic defect-generation kinetics and effective NIEL in GaN," *IEEE Trans. Nucl. Sci.*, vol. 65, no. 5, pp. 1108–1118, Apr 2018.

[14] K. Nordlund *et al.*, "Primary radiation damage: A review of current understanding and models," *Phys. Rev. B*, vol. 512, pp. 450–479, Dec 2018.

[15] C. S. Miguel *et al.*, "Unravelling the secrets of the resistance of GaN to strongly ionising radiation," *Nat. Comm.*, vol. 4, no. 1, Mar 2021, Art. no. 51.

[16] M. O. Ruault and W. Jäger, "Transmission electron microscope investigations of defects produced by individual displacement cascades in Si and Ge," *J. Micro.*, vol. 118, no. 1, pp. 67–73, Jan 1980.

[17] L. Howe and M. Rainville, "Features of collision cascades in silicon as determined by transmission electron microscopy," *Nucl. Instr. Meth.*, vol. 182-183, pp. 143–151, May 1981.

[18] D. Lambert *et al.*, "Neutron displacement damage cross-section in GaN: numerical evaluations and differences with Si," *IEEE Trans. Nucl. Sci.*, vol. 70, no. 8, pp. 1870–1877, Apr 2023.

[19] M. Raine *et al.*, "Simulation of single particle displacement damage in silicon – Part I: Global approach and primary interaction simulation," *IEEE Trans. Nucl. Sci.*, vol. 64, pp. 133–140, Oct 2017.

[20] A. Jay *et al.*, "Simulation of single particle displacement damage in silicon–Part II: Generation and long-time relaxation of damage structure," *IEEE Trans. Nucl. Sci.*, vol. 64, pp. 141–148, Nov 2017.

[21] A. Jay, *et al.*, "Simulation of single particle displacement damage in silicon–Part III: First principle characterization of defect properties," *IEEE Trans. Nucl. Sci.*, vol. 65, pp. 724–731, Jan 2018.

[22] G. Herrero-Saboya *et al.*, "A comprehensive theoretical picture of e centers in silicon: From optical properties to vacancy-mediated dopant diffusion," *J. App. Phys.*, vol. 127, no. 8, Feb 2020, Art. no. 085703.

[23] T. Jarrin *et al.*, "Simulation of single particle displacement damage in $Si_{1-x}Ge_x$ alloys - interaction of primary particles with the material and generation of the damage structure," *IEEE Trans. Nucl. Sci.*, vol. 67, no. 7, pp. 1273–1283, Jan 2020.

[24] T. Jarrin, *et al.*, "Parametric study of the two-temperature model for molecular dynamics simulations of collision cascades in Si and Ge," *Nucl. Instr. Meth. Phys. R. B*, vol. 485, pp. 1–9, Dec 2020.

[25] S. Plimton, "Fast parallel algorithms for short-range molecular dynamics," *J. Comput. Phys.*, vol. 117, pp. 1–19, Mar 1995.

[26] D. Frenkel and B. Smit, *Understanding Molecular Simulation*. San Diego, USA: Academic Press, 2002.

[27] K. Nordlund *et al.*, "Defect production in collision cascades in elemental semiconductors and FCC metals," *Phys. Rev. B*, vol. 57, no. 13, pp. 7556–7570, Apr 1998.

[28] A. Béré and A. Serra, "Atomic structure of dislocation cores in GaN," *Phys. Rev. B*, vol. 65, May 2002, Art. no. 205323.

[29] J. F. Ziegler, J. P. Biersack, and U. Littmark, *The stopping range of ions in solids*, 1st ed. NY, USA: Pergamon Press, 1983.

[30] J. Tersoff, "New empirical approach for the structure and energy of covalent systems," *Phys. Rev. B*, vol. 37, pp. 6991–7000, Apr 1988.

[31] R. Devanathan *et al.*, "Displacement threshold energies in β-SiC," *J. Nucl. Mat.*, vol. 253, no. 1, pp. 47–52, Mar 1998.

[32] J. Tersoff, "Modeling solid-state chemistry: Interatomic potentials for multicomponent systems," *Phys. Rev. B*, vol. 39, pp. 5566–5568, Mar 1989.

[33] S. Corporation, "fix electron/stopping command," 2023. [Online]. Available: https://docs.lammps.org/fix_electron_stopping.html Accessed on : July 2023

[34] T. Jarrin *et al.*, "Coping with the stochasticity of collision cascades in molecular dynamics simulations," *Nucl. Instr. Meth. Phys. R. B*, vol. 500-501, pp. 1–9, Aug 2021.

[35] H. Hensel and H. M. Urbassek, "Implantation and damage under low-energy Si self-bombardment," *Phys. Rev. B*, vol. 57, Feb 1998, Art. no. 4756.

[36] P. F. Zou and R. F. W. Bader, "A topological definition of a Wigner–Seitz cell and the atomic scattering factor," *Acta Crist. A*, vol. 50, no. 6, pp. 714–725, Nov 1994.

[37] A. Stukowski, "Visualization and analysis of atomistic simulation data with ovito–the open visualization tool," *Modelling and simulation in materials science and engineering*, vol. 18, no. 1, 2009, Art. no. 015012.

[38] J. F. Ziegler, M. D. Ziegler, and J. P. Biersack, "SRIM - The stopping and range of ions in matter (2010)," *Nucl. Instr. Meth. Phys. R. B*, vol. 268, pp. 1818–1823, Jun 2010.

[39] P. Lopez *et al.*, "Molecular dynamics simulations of damage production by thermal spikes in Ge," *J. App. Phys.*, vol. 111, Feb 2012, Art. no. 033519.

[40] W. Haynes, *CRC Handbook of Chemistry and Physics*. Boca Raton, USA: CRC Press.

[41] J. R. Srour and J. W. Palko, "Displacement damage effects in irradiated semiconductor devices," *IEEE Trans. Nucl. Sci.*, vol. 60, pp. 1740–1766, Jun 2013.

[42] A. Jeżowski *et al.*, "Thermal conductivity of GaN crystals in 4.2–300 K range," *Sol. St. Comm.*, vol. 128, no. 2, pp. 69–73, Jan 2003.

[43] E. Holmström *et al.*, "Threshold defect production in silicon determined by density functional theory molecular dynamics simulations," *Phys. Rev. B*, vol. 78, Jul 2008, Art. no. 045202.

[44] E. Holmstrom, K. Nordlund, and A. Kuronen, "Threshold defect production in germanium determined by density functional theory molecular dynamics simulations," *Phys. Scr.*, vol. 81, Mar 2010, Art. no. 035601.